The Astrophysical Journal, 813:100 (9pp), 2015 November 10 doi:10.1088/0004-637X/813/2/100

DEEP *GALEX* UV SURVEY OF THE *KEPLER* FIELD. I. POINT SOURCE CATALOG

Manuel Olmedo[1,2], James Lloyd[3,4], Eric E. Mamajek [2], Miguel Chávez[1], Emanuele Bertone[1], D. Christopher Martin[5], and James D. Neill[5]
[1] Instituto Nacional de Astrofísica Optica y Electrónica Luis Enrique Erro #1, CP 72840, Tonantzintla, Puebla, Mexico; olmedo@inaoep.mx
[2] University of Rochester, Department of Physics & Astronomy, Rochester, NY 14627-0171, USA
[3] Department of Astronomy, Cornell University, Ithaca, NY, USA
[4] Carl Sagan Institute and Cornell Center for Astrophysics and Planetary Science, Cornell University, Ithaca, NY, USA
[5] California Institute of Technology, 1200 East California Boulevard, MC 278-17, Pasadena, CA 91125, USA
Received 2015 May 18; accepted 2015 October 1; published 2015 November 3

ABSTRACT

We report observations of a deep near-ultraviolet (NUV) survey of the *Kepler* field made in 2012 with the *Galaxy Evolution Explorer* (*GALEX*) Complete All-Sky UV Survey Extension (CAUSE). The *GALEX*-CAUSE *Kepler* survey (GCK) covers 104 square degrees of the *Kepler* field and reaches a limiting magnitude of NUV $\simeq$ 22.6 at 3σ. Analysis of the GCK survey has yielded a catalog of 669,928 NUV sources, of which 475,164 are cross-matched with stars in the *Kepler* Input Catalog. Approximately 327 of 451 confirmed exoplanet host stars and 2614 of 4696 candidate exoplanet host stars identified by *Kepler* have NUV photometry in the GCK survey. The GCK catalog should enable the identification and characterization of UV-excess stars in the *Kepler* field (young solar-type and low-mass stars, chromospherically active binaries, white dwarfs, horizontal branch stars, etc.), and elucidation of various astrophysics problems related to the stars and planetary systems in the *Kepler* field.

Key words: catalogs – stars: activity – stars: chromospheres – techniques: photometric – ultraviolet: stars

Supporting material: machine-readable tables

1. INTRODUCTION

The fast growth of exoplanet detections has motivated the derivation of more accurate fundamental stellar properties (e.g., mass, radius, age, etc.) and the connection between these properties and those of their evolving planetary systems. The precision with which the exoplanets' parameters can be estimated directly depends on the precision associated with the properties of their stellar hosts. Of particular importance is the stellar age, since one of the major goals in the study of exoplanetary systems is to establish their evolutionary stage, and how this compares to the properties of our own solar system.

Reliably age-dating solar-type field stars is notoriously difficult. For these stars, alternative methods to isochrone fitting techniques have been explored. Chromospheric activity and stellar rotation are among the more reliable observables for stellar age estimation of Sun-like main sequence stars. The most common and accessible proxy for stellar activity has been the emission in the Ca II resonance line in the optical-ultraviolet spectral interval (e.g., Mamajek & Hillenbrand 2008). Alternative proxies have also been identified and include the high contrast emission of Mg II line in the ultraviolet (UV) and the continuum UV excess (e.g., Findeisen et al. 2011; Olmedo et al. 2013). For these stars, UV radiation originates in the hot plasma of the upper stellar atmospheres at temperatures of $\sim 10^4$–10^6 K, heated by non-thermal mechanisms, such as acoustic and magnetic waves, generated by convection and rotation (e.g., Narain & Ulmschneider 1996; Ulmschneider et al. 2003). As the star ages, it loses angular momentum due to magnetic braking (Mestel 1968; Kawaler 1988), slowing the rotation and affecting the stellar dynamo, which in turn decreases the magnetic field leading to a decrement of the UV emission. In this first paper of a series aimed at investigating the UV properties of stars, we present a complete catalog of UV sources detected by the *Galaxy Evolution Explorer* (*GALEX*; Martin et al. 2005; Bianchi et al. 2014) in the field of the *Kepler* Mission (Basri et al. 2005).

The *Kepler* field (i.e., the 100 square degree field of the original *Kepler* mission) has been fully surveyed at different optical and infrared bandpasses (Lawrence et al. 2007; Brown et al. 2011; Everett et al. 2012; Greiss et al. 2012). Its stellar content, mainly comprised of field stars, with over 450 confirmed [6] exoplanet host stars, has rapidly become one of the most studied stellar samples and regions of the sky. The *Kepler* field and associated survey data comprise a potentially valuable resource for studying the age-activity-rotation relation for low-mass stars. Rotation periods (and ages) of stars in the *Kepler* field have been determined in a number of studies (e.g., Reinhold et al. 2013; Walkowicz & Basri 2013; do Nascimento et al. 2014; García et al. 2014; McQuillan et al. 2014; Meibom et al. 2015).

The *GALEX* UV space observatory was launched in 2003 and was operated by NASA until 2011 (Martin et al. 2005; Bianchi et al. 2014). Afterwards, the *GALEX* mission was managed by Caltech for about a year as a private space observatory, until the satellite was turned off in June 2013. *GALEX* is a 50 cm Ritchey–Chrétien telescope with a 1°.25 wide field of view, equiped with a near-UV (NUV; 1771–2831 Å, $\lambda_{\rm eff} = 2271$ Å) and a far-UV (FUV; 1344–1786 Å, $\lambda_{\rm eff} = 1528$ Å) detectors. During its main mission, *GALEX* carried out the All-Sky, Medium, and Deep Imaging Surveys, with exposure times of $\sim$100, $\sim$1000, and >10,000 s, respectively, measuring more than 200 million sources (Bianchi et al. 2014). The continuation phase, called the *GALEX* Complete All-Sky UV Survey Extension (CAUSE), was funded by several consortia, with the main goal of extending observations in the NUV band to the Galactic plane, which was only scarcely

[6] http://kepler.nasa.gov/ as of 2015 September 11.

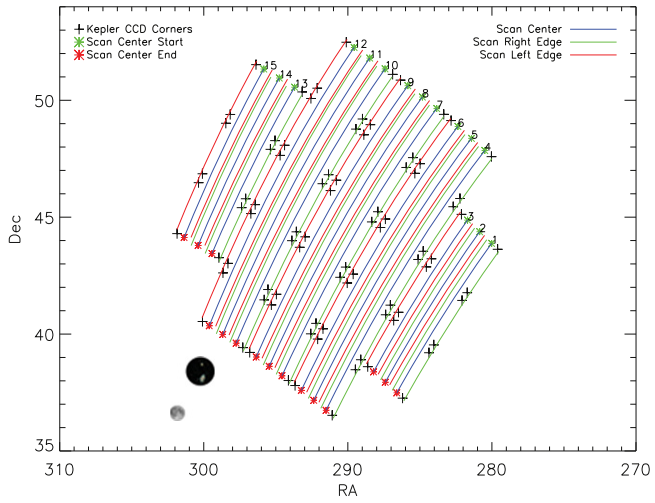

Figure 1. Scan mode observations of GCK survey covering the *Kepler* field. The field of view of *GALEX* and a full moon are shown for comparison. The numbers on the upper right edges correspond to the scan numbers. The plus symbols corresponds to the edges of *Kepler* detectors.

Table 1
Files of GCK data set

Fits name	Image type	Units
nd-count.fits	count image	photons/pix
nd-rrhr.fits	effective exposure map	s pix^{-1}
nd-int.fits	intensity map	photons s^{-1} pix^{-1}
nd-flags.fits	artifact flags image	⋯
xd-mcat.fits	catalog of sources	⋯

mapped during the main mission, due to restrictions on the maximum target brightness.

In this work, we describe the creation of a deep NUV photometric catalog with nearly full coverage of the *Kepler* field using CAUSE observations. In Section 2 we introduce the observations and characteristics of the data. In Section 3 we explain the procedure for extracting the NUV point sources. Section 4 describes the point source catalog, and its crossmatch with the *Kepler* Input Catalog (KIC) and the *Kepler* Objects of Interest (KOI) catalog is presented in Section 5. Finally, the publicly available *GALEX*-CAUSE (GCK) catalog of NUV sources is described in Section 6.

2. OBSERVATIONS

As part of the CAUSE survey, Cornell University funded 300 orbits to complete the spatial coverage of the *Kepler* field through 2012 August–September (PI J. Lloyd). The data set of GCK field observations is composed of 180 tiles that cover the *Kepler* field (Borucki et al. 2003; Basri et al. 2005; Brown et al. 2005; Latham et al. 2005); each tile has 20 visits on average. These observations sample timescales from a millisecond to a month, and can be used to identify variable targets and exotic sources on such timescales. The GCK data set provides spatial coverage of the *Kepler* field in the *GALEX* NUV band.

The standard *GALEX* pointed observation mode adopted for the surveys during the primary NASA *GALEX* mission employed a 1.′5 spiral dither pattern. This dither moves the sources with respect to detector artifacts and prevents a bright source to saturate one position on the detector, which is subject to failure if overloaded. The *GALEX* data pipeline processes the photon arrival times and positions with an attitude solution that reconstructs an image of the sky for a single tile, 1.°2 in diameter around the pointing center.

In 2012, a drift mode was adopted, which scanned a strip of the sky along a great circle. For GCK observations, these scans run as long as 12°. The scan mode processing uses a pipeline adapted from the pointed mode observations.[7] To adapt the scans to the standard tile processing pipeline, they are processed in tile sized images resulting in 9 and 14 images for the short scans (1−3 and 13−15) and long scans (4−12), respectively (shown in Figure 1). Thus for the 180 tiles of the GCK data, with each visited an average of 20 times, we have a total of ∼3200 images.

The GCK data were processed with the *GALEX* scan-mode pipeline and subsequently delivered to Cornell in the form of packs of 5 images (see Table 1 for details) per visit for each tile. For details on these files or any technical information concerning the *GALEX* mission, see http://www.galex.caltech.edu/wiki/Public:Documentation.

A mosaic of the *GALEX* CAUSE NUV observations is shown on Figure 2. The superimposed blue box corresponds to the central CCD of the *Kepler* detector array. Most of the data exhibit the exquisite photometric and astrometric stability and reproducibility expected for a space observatory. However, the *GALEX* pipeline failed to correctly process a small fraction of the images. A thorough visual inspection showed that there are about 450 images affected by doubling or ghosting of sources. An example of this effect is illustrated in Figure 3. All these images were excluded from our analysis.

The final exposure time map is presented in Figure 4. Some tiles lack a single good visit and are located at the end of a scan, when the spacecraft was executing a maneuver. Because of this, the 13th image of scans 4, 5, 6, 9, and 10 were not included in the catalog construction (leaving a total of 175 tiles), representing a loss of no more than 0.5% coverage of the *Kepler* field. Within the main *GALEX* surveys, fractions of the *Kepler* field were partially surveyed (Smith et al. 2011). A cumulative distribution of the exposure time in function of sky coverage is shown in Figure 5 (solid blue line), and the orange dashed line corresponds to the *GALEX* release 6 (GR6).

3. ASSEMBLY OF A CATALOG OF NUV SOURCES

The construction of the GCK catalog can be summarized in four stages, each of which is discussed in this section. In the first stage, "Image Co-adding," the available single epoch visits for each tile are co-added. Next, the "Background Estimation" is carried out from the intensity image using a modified σ-κ clipping method. The "Source Extraction and Photometry" uses the software SExtractor (Bertin & Arnouts 1996) to first detect and then perform photometry on the background-subtracted intensity image for each tile obtained in the previous stage. In the final stage the catalogs from each of the 175 tiles are combined, and duplicate objects, low signal-to-noise ratio (S/N) sources, and other possible spurious sources are carefully removed.

[7] http://galex.stsci.edu/GR6/?page=scanmode

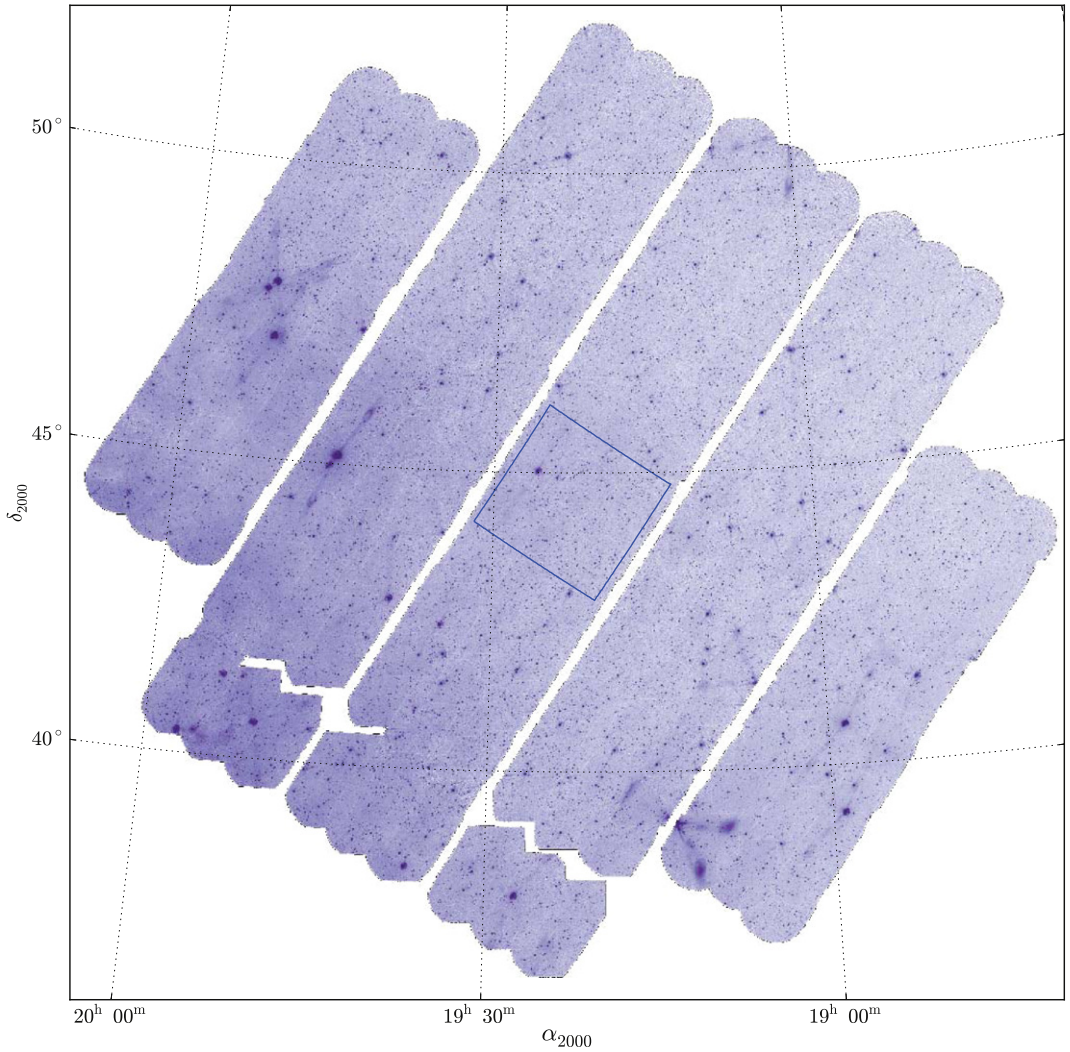

Figure 2. Intensity image mosaic of *GALEX* CAUSE NUV observations. The blue square corresponds to the central CCD of the *Kepler* telescope.

Figure 3. *GALEX* image corresponding to scan 1, image 2, visit 2, as an example of a failure of the pipeline processing: bright sources appear as double objects.

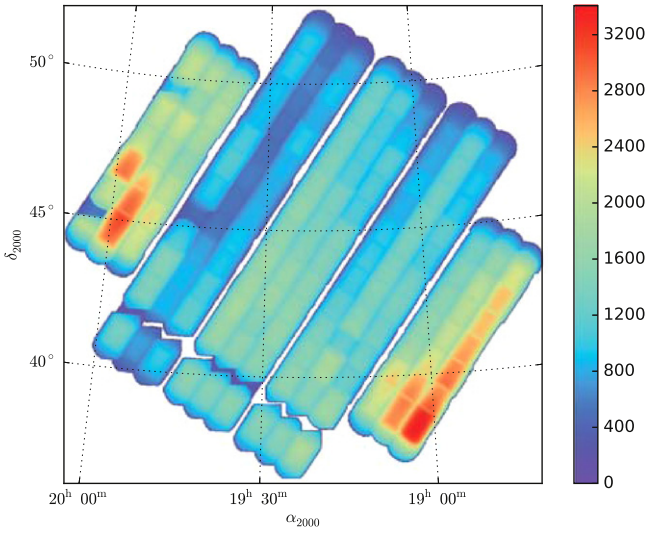

Figure 4. Mosaic of the effective exposure time of the *GALEX* CAUSE observations.

3.1. Image Co-adding

Prior to co-adding all epochs for a given tile, each image was visually inspected, discarding visits presenting the source doubling or ghosting issue (Figure 3). Since the images already have an astrometric solution, and furthermore, each epoch for a given tile are aligned, co-adding only requires an arithmetic sum. For each tile, the process was as follows.

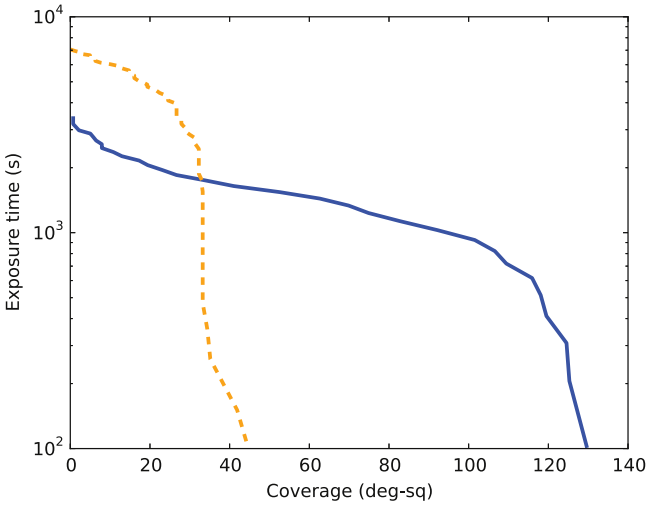

Figure 5. Cumulative distributions of exposure time of the sky coverage of the GCK *Kepler* field (solid blue line). Observations from the *GALEX* release 6 (GR6) are represented with the dashed orange line.

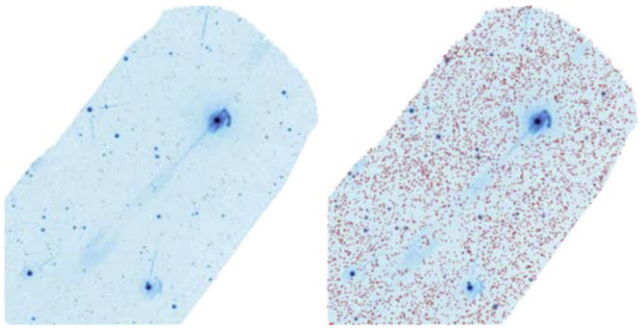

Figure 6. *Left panel*: co-added intensity image for image 6 of scan 2. *Right panel*: the same image with source detected marked as red points. Note the absence of detection in the area affected by instrumental artifacts.

Table 2
Artifact Flags

Number	Short name	Description
1(1)	edge	Detector bevel edge reflection (NUV only)
2(2)	window	Detector window reflection (NUV only)
3(4)	dichroic	Dichroic reflection
4(8)	varpix	Variable pixel based on time slices
5(16)	brtedge	Bright star near field edge (NUV only)
6(32)	detector rim	Proximity(>0.6 degrees from field center)
7(64)	dimask	Dichroic reflection artifact mask flag
8(128)	varmask	Masked pixel determined by varpix
9(256)	hotmask	Detector hot spots
10(512)	yaghost	Possible ghost image from YA slope

Note. From the *GALEX* documentation, chapter 8 (http://www.galex.caltech.edu/wiki/Public:Documentation/Chapter_8). Artifacts 7, 8, 9 do not apply to the the GCK catalog.

1. Construction of the co-added count image as the arithmetic sum of individual count intensity images (*nd-count.fits*).
2. Construction of the co-added effective exposure image as the arithmetic sum of individual effective exposure images (*nd-rrhr.fits*).
3. Construction of a combined flag image as the logic OR of the individual flag images (*nd-flags.fits*).

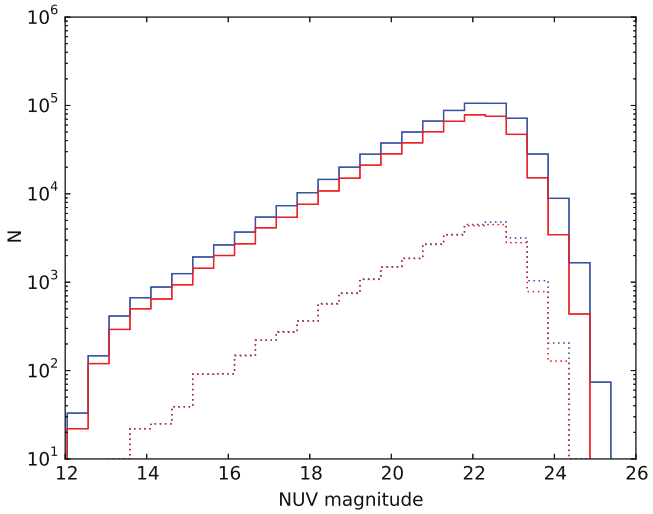

Figure 7. Distribution of NUV detections. Blue line is the distribution of objects on the GCK catalog, red line are the matched objects with the KIC. Dotted lines correspond to a sample of detections inside a the sky region defined on Figure 2.

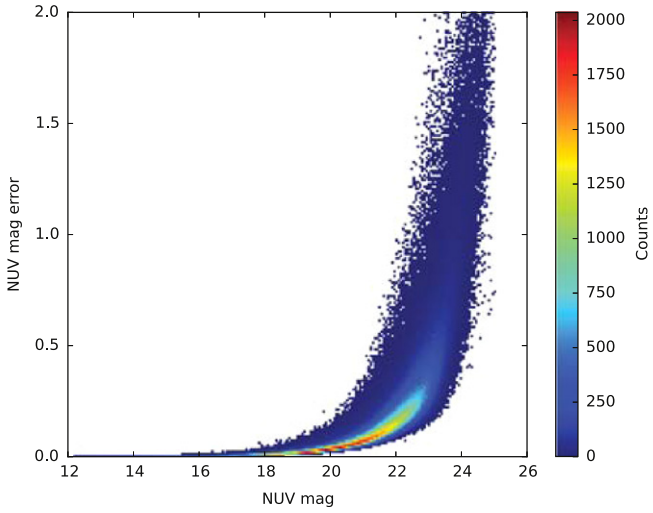

Figure 8. NUV photometric error distribution for the GCK catalog. The color scale indicates the density of the sources in the plot.

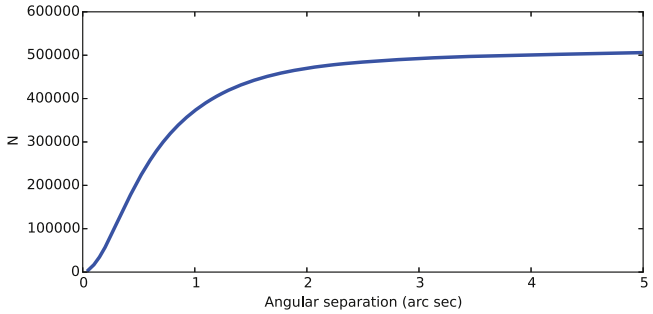

Figure 9. Cumulative distributions of separations of the GCK—KIC cross-match.

4. Calculation of the the ratio of the co-added count and effective exposure images to obtain the final intensity image.

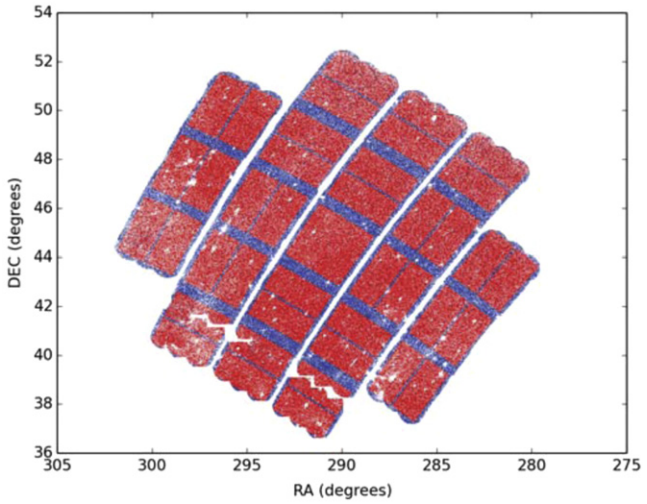

Figure 10. Spatial distribution of the GCK sources in the *Kepler* field. Red dots indicate GCK sources with a counterpart in the KIC, while blue dots mark GKC sources without a KIC match. The saw-like regions in the south-east show the tile that were lost due to the pipeline failure (see Section 2). Small circular empty regions are due to very bright stars, whose surrounding artifacts compromised nearby sources detections.

3.2. Background and Threshold Estimations

The source extraction and photometry methodology follows that of the *GALEX* pipeline (reported in Morrissey et al. 2007).[8] Prior to this step, background and threshold images are built, as required by SExtractor.

Background estimation: the construction of a background image consists of an iterative σ-κ clipping method. The *count* image is divided into square bins 128 pix wide. In each bin, the local background histogram is built using the Poisson distribution (due to the low NUV background count rates), and the probability $P_k(x)$ of observing k events for a mean rate x is calculated. Pixels with a $P_k(x) < 1.35 \times 10^{-3}$ (equivalent to a 3σ level) are iteratively clipped until convergence is reached. Then a 5×5 pix median filter is applied to decrease the bias by bright sources. The bin mesh is upsampled to the original resolution and divided by the effective exposure image to produce the final *background* image, which is subtracted from the *intensity* image to produce the *background-subtracted intensity* image.

Weight threshold image: this image provides the threshold for potential detections. The *count* image is again divided in 128×128 pix bins. In each bin the value of k, in counts/pix, which corresponds to probability level of 3σ is computed and stored to produce a threshold map. This map is upsampled to the original resolution and divided by the effective exposure image, in order to obtain a threshold image in counts s^{-1} pix^{-1}. The final step is to compute a *weight threshold* image by dividing the *background-subtracted intensity* image by this last threshold image.

3.3. Source Extraction and Photometry

The detection and photometry process is carried out with SExtractor working in dual mode: the *weight threshold* image is used for detecting sources, while their photometry is computed on the *background-subtracted intensity* image. The SExtractor parameters *THRESH_TYPE* and *DETECT_THRESH* are set to "absolute" and "1"; in this way, SExtractor will consider all pixels with values above 1 in the *weight threshold* image as possible detections. SExtractor is executed for each of the 175 tiles in the GCK data, delivering detection and photometry of each source. The photometric error *dm* in magnitude is calculated following the *GALEX* pipeline[9]

$$df = \frac{\sqrt{(f + s\Omega)t}}{t}, \qquad dm = 1.086 \cdot df/f, \tag{1}$$

where f is the flux from the source in counts s^{-1}, s is the sky level in counts s^{-1} pix^{-1}, Ω is the area over which the flux is measured, and t is the effective exposure time in seconds.

3.4. Artifact Identification

In the *GALEX* imagery, there are various artifacts, not all of which are automatically detected by the *GALEX* pipeline. The worrisome non-flagged artifacts are large diffuse reflections within the field surrounding very bright stars. The shapes of these artifacts have quite different morphologies, however, the most common shapes are long thin cones, halos, and horse-shoe-shaped extended reflections. An example is shown in Figure 6. These artifacts bias the background and affect source detection, mainly producing false positives.

3.4.1. False Positives

In order to remove extended objects and spurious detections, caused by non-flagged artifacts in the images, we design suitable criteria to remove them, while at the same time minimizing the loss of genuine sources. The criteria were defined considering the geometric characteristics of the aperture fitted by SExtractor to the flux profile of detection and the S/N:

1. Semiminor axis $> 60''$;
2. Eccentricity > 0.95;
3. S/N < 1.05;
4. S/N < 1.5 and Semimajor axis $> 10''$.

The first two criteria are intended to remove large and/or extended sources, including false detections inside extended artifacts. The third criteria discards too low S/N detections, while the purpose of the fourth criteria is to remove detections at the border of images, where the flux inside the SExtractor apertures may not be reliable. We defined the above thresholds through a trial and error process, aimed at discarding most of the false positives, while minimizing the loss of real sourcesones. The right panel of Figure 6 shows the source detections after removing false positives.

3.4.2. Artifact Flags

The *GALEX* pipeline produces a *flag* image for each tile. This image marks the pixels where the intensity image is affected by some artifacts or where artifacts were removed. Each detected source has the *artifact_flags* keyword, that is a logical OR of the artifact flags for pixels that were used to compute its photometry. These flags are summarized in Table 2. The flags were developed for the dither mode observations and in some cases are not directly applicable to the scan mode

[8] http://www.galex.caltech.edu/wiki/Public:Documentation/Chapter_104

[9] Section 4 from: http://asd.gsfc.nasa.gov/archive/galex/Documents/GALEXPipelineDataGuide.pdf

Table 3
GCK Catalog Tags

Tag Number	Tag Name	Description	Unit
1	gck_id	*GALEX* CAUSE *Kepler* (GCK) Identifier	number
2	alpha_j2000	Right ascension	Decimal degrees
3	delta_j2000	Declination	Decimal degrees
4	nuv_mag	Calibrated NUV magnitude	AB magnitude
5	nuv_magerr	Error of the calibrated NUV magnitude	AB magnitude
6	nuv_mag_cor	Corrected calibrated NUV magnitude with Camarota & Holberg (2014) calibration	AB magnitude
7	nuv_magerr_cor	Error of the corrected calibrated NUV magnitude	AB magnitude
8	nuv_flux	NUV flux	counts s^{-1}
9	nuv_fluxerr	Error of NUV flux	counts s^{-1}
10	nuv_s2n	Signal-to-noise ratio of NUV flux	dimensionless
11	nuv_bkgrnd_mag	NUV background surface brightness at source position	AB magnitude
12	nuv_bkgrnd_flux	Background NUV flux at source position	counts s^{-1} $arcsec^{-2}$
13	nuv_exptime	Effective exposure time at source position	s
14	fov_radius	Distance of source from center of tile	degrees
15	artifact_flags	Logical OR of artifact flags	number
16	ktswckey	Sequential number in CasJobs *Kepler* Colors Table of match	number
17	kic_keplerid	*Kepler* Input Catalog identifier of match	number
18	scan	GCK scan number	dimensionless
19	image	GCK image number	dimensionless
20	kep_name	*Kepler* host star name	dimensionless
21	kic_kepmag	*Kepler*-band magnitude	AB magnitude
22	kic_g	g-band Sloan magnitude from the *Kepler* Input Catalog	AB magnitude
23	kic_r	r-band Sloan magnitude from the *Kepler* Input Catalog	AB magnitude
24	kic_i	i-band Sloan magnitude from the *Kepler* Input Catalog	AB magnitude
25	kic_z	z-band Sloan magnitude from the *Kepler* Input Catalog	AB magnitude
26	twomass_j	2MASS J-band magnitude	Vega magnitude
27	twomass_h	2MASS H-band magnitude	Vega magnitude
28	twomass_k	2MASS K-band magnitude	Vega magnitude

observations. For example, in dither mode observations, only the outer region of any field is close to the detector edge, but in scan mode the detector edge crosses nearly the entire field for a fraction (but only a fraction) of the integration. The detector edge proximity flag (Flag 6) is therefore set by the pipeline, but it does not induce errors in the data quality. Flags 1 and 5 indicate the possible presence of reflections near the edge of the FOV. However, we have found that in many instances the regions affected by this latter artifact do not actually show any obvious problem. We therefore consider Flag 1 and 5 as non influential. Detections with flags 2, 3, and 10 have been discarded because their photometry is affected by an unreliable background level determination. An example of an image which presents regions marked by the flag 3, the dichroic reflection, is shown in Figure 6, where one can distinguish arc-shaped features around the three brightest stars in the image.

The *GALEX* pipeline flags were developed for the dither mode observations and in some cases are not directly applicable to the scan mode observations in the same way as the dither mode observations. For example, in dither mode only the outer region of any field is close to the detector edge, but in scan mode the detector edge crosses nearly the entire field for a fraction (but only a fraction) of the integration. The detector edge proximity flag is therefore set by the pipeline, but it does not induce errors in the data quality.

4. THE GCK UV SOURCE CATALOG.

After processing each file through false positive removal and flagging, the 175 catalogs are combined to produce a single point source catalog for the whole GCK field. In the case of sources with multiple detections (due to small overlap between tiles), the measurement with the highest S/N was retained.

The resulting GCK catalog contains 660,928 NUV sources. The NUV brightness distribution of the GCK sources is shown in Figure 7 (blue lines), while the photometric error is plotted in Figure 8. One can see that a typical error for sources with NUV < 22.6 mag is less than 0.3 mag.

The GCK Catalog includes a few thousand objects with NUV $\lesssim 15.5$, whose flux estimation is affected by the non-linearity of the *GALEX* NUV detector (discussed by Morrissey et al. 2007). The magnitude of this nonlinearity effect can be as large as $\sim$1.0 mag at NUV $\simeq$ 12 mag. In a recent analysis of the *GALEX* absolute calibration, Camarota & Holberg (2014) identified a nonlinear correlation when comparing *GALEX* data of an extend sample of white dwarf stars with predicted magnitudes from model atmospheres and spectroscopic data collected by the *International Ultraviolet Explorer* (*IUE*). They provide a correction that properly converts the *GALEX* NUV magnitudes to the *Hubble Space Telescope* photometric scale. We applied this correction, based on the data in Table 3[10] of Camarota & Holberg (2014), to all GCK stars with NUV $\leqslant$ 15.71 mag, for which we also provide the original *GALEX* magnitudes. We also obtain an uncertainty of 0.22 mag, associated with the magnitude conversion, by computing the standard deviation of the Camarota & Holberg (2014) data with respect to their best fit.

[10] Note that the correct C0 coefficient is 14.0821 for the *IUE* synthetic fluxes (L.Camarota 2015 private communication).

Table 4
GCK Catalog Sample

	Column																	
(1)	(2)	(3)	(4)	(5)	(6)	(7)	(8)	(9)	(10)	(11)	(12)	(13)	(14)	(15)	(16)	(17)	(18)	(19)
GCK J18461428 +4420359	281.55948	44.34330	23.768	0.638	−999	−999	0.033	0.02	1.7	26.95	0.002	1013.0	0.843	32	792984	8344414	2	2
GCK J19531681 +4926274	298.32004	49.44096	20.854	0.072	−999	−999	0.490	0.03	15.1	26.15	0.004	1262.5	0.754	32	None	None	15	4
GCK J19325850 +4922011	293.24375	49.36697	20.038	0.055	−999	−999	1.040	0.05	19.8	26.60	0.002	692.6	0.497	17	None	None	12	5
GCK J19432870 +3909313	295.86958	39.15869	14.803	0.003	14.681	0.220	129.076	0.35	366.7	25.79	0.005	1101.0	0.661	48	658168	4075067	9	14
GCK J19183283 +3827439	289.63681	38.46219	22.907	0.285	−999	−999	0.074	0.02	3.8	26.34	0.003	1524.7	0.596	1	12145669	None	4	12
GCK J19145926 +4453507	288.74693	44.89742	22.893	0.369	−999	−999	0.075	0.03	2.9	26.52	0.003	1372.3	0.197	4	4369546	8681571	7	7
GCK J19503417 +4804597	297.64238	48.08325	22.789	0.251	−999	−999	0.083	0.02	4.3	26.01	0.004	1593.2	0.625	32	15256924	None	14	5
GCK J19290783 +4543284	292.28261	45.72457	20.826	0.093	−999	−999	0.503	0.04	11.7	26.48	0.003	611.5	0.657	32	None	None	10	7
GCK J19550979 +4151533	298.79079	41.86481	19.239	0.037	−999	−999	2.170	0.07	29.3	25.64	0.006	875.6	0.739	32	6369109	6469387	12	14
GCK J19523858 +4422221	298.16074	44.37282	16.702	0.006	−999	−999	22.440	0.12	193.2	25.98	0.004	1819.6	0.415	20	14957236	None	13	8

Note. Column number correspond to tag number in Table 3. A −999 value indicates unavailable datum.

(This table is available in its entirety in machine-readable form.)

Table 5
NUV Magnitudes and Ancillary Data for *Kepler* Targets with Confirmed Exoplanets

								Column									
(17)	(20)	(1)	(2)	(3)	(4)	(5)	(6)	(7)	(10)	(21)	(22)	(23)	(24)	(25)	(26)	(27)	(28)
8359498	*Kepler*-77	GCK J19182585 +4420438	289.60772	44.34550	20.575	0.056	−999	−999	19.43	13.938	14.449	13.871	13.720	13.658	12.757	12.444	12.361
8644288	*Kepler*-18	GCK J19521905 +4444474	298.07939	44.74650	20.842	0.062	−999	−999	17.62	13.549	14.160	13.479	13.287	13.187	12.189	11.872	11.756
6616218	*Kepler*-314	GCK J19384180 +4204320	294.67418	42.07566	19.777	0.035	−999	−999	31.03	12.557	13.126	12.459	12.313	12.205	11.242	10.849	10.778
9821454	*Kepler*-59	GCK J19080950 +4638249	287.03957	46.64025	19.263	0.026	−999	−999	41.77	14.307	14.669	14.259	14.152	14.116	13.253	12.974	12.928
9595827	*Kepler*-71	GCK J19392762 +4617097	294.86508	46.28602	21.969	0.226	−999	−999	4.80	15.127	15.692	15.061	14.885	14.803	13.926	13.550	13.468
9884104	*Kepler*-219	GCK J19145734 +4645455	288.73890	46.76264	19.609	0.031	−999	−999	35.27	13.764	14.174	13.692	13.588	13.537	12.678	12.400	12.388
11121752	*Kepler*-380	GCK J18493471 +4845327	282.39464	48.75907	18.278	0.031	−999	−999	35.46	13.652	14.047	13.614	13.483	13.464	12.614	12.349	12.288
2302548	*Kepler*-261	GCK J19252754 +3736322	291.36477	37.60894	21.181	0.143	−999	−999	7.58	13.562	14.271	13.495	13.259	13.118	12.127	11.672	11.585
8572936	*Kepler*-34	GCK J19454460 +4438294	296.43583	44.64151	20.884	0.089	−999	−999	12.25	14.875	15.372	14.830	14.662	14.575	13.605	13.301	13.237
6850504	*Kepler*-20	GCK J19104751 +4220188	287.69795	42.33856	18.900	0.019	−999	−999	56.16	12.498	12.997	12.423	12.284	12.209	11.252	10.910	10.871

Note. Column number correspond to tag number in Table 3. A −999 value indicates an unavailable datum.

(This table is available in its entirety in machine-readable form.)

5. CROSSMATCH WITH KIC AND KOI

The positions of the GCK objects were cross-matched with the KIC (Brown et al. 2011), using a 2.″5 search radius. This value is compatible with the astrometric precision of *GALEX* observations, extending the crossmatch beyond this radius does not increase the number of matches more than 1%, as can be seen in the Figure 9. The cross-match resulted in 475,164 GCK objects with KIC counterparts. We would like to remark that a smaller search radius would significantly decrease the number of detections, while a larger radius would only increase the KIC sources to be associated with a single NUV source. In the final catalog we provide the identification of KIC counterparts.

The spatial location of these objects are plotted as red points in Figure 10, where they obviously coincide with the position of the *Kepler* satellite detectors. Their NUV brightness distribution is also shown in Figure 7. The constant ratio difference (up to NUV $\sim$ 22.5 mag) between the GCK and KIC distributions seen in Figure 7 is due to incomplete coverage of the *Kepler* field (caused by the gaps between the *Kepler* mission detectors (Figure 10). In order to avoid this issue, we also show in Figure 7 the number distribution of GCK sources and their KIC counterparts of the objects on the central *Kepler* detector (see Figure 2); we can see that almost all GCK sources have KIC counterparts up to NUV $\sim$ 22.5 mag.

We also cross-matched the GCK catalog with the KOI catalog available in MAST through the tool CasJobs[11], and found 2614 candidate host stars (hosting 3390 planets) in common and 327 stars (hosting 768 planets) among the *Kepler* Confirmed Planets hosts. The GCK catalog should enable investigation of the UV excess as a function of stellar age, rotation, and metallicity, identification of UV-bright (potentially young) stars, and provide UV photometry for other astrophysically interesting systems in the *Kepler* field.

6. DESCRIPTION OF THE CATALOG FILE

Table 3 provides the description of the fields in the GCK catalog file (columns 1–19). The first keyword is the *gck_id*, the main identifier of the GCK catalog, with a sexagesimal, equatorial position-based source name (i.e., GCK Jhhmmss.ss +ddmmss.s). The second and third keywords are the coordinates of the NUV detection. The following keywords give the photometry in magnitudes and fluxes, with their corresponding errors. The keyword *artifacts_flags* provides the flags described in Table 2. For objects with a cross-match in the KIC the keywords *ktswckey* and *kic_keplerid*, are provided for the nearest counterpart. The keyword *ktswckey* is particularly useful to get data from the table *keplerObjectSearchWithColors*, also available in MAST through the tool CasJobs. This table contains the KIC catalog and other catalogs with coverage of the *Kepler* field. In Table 4, we show a portion of the GCK catalog. The column tags designates the keyword number that also appear in Table 3. The GCK catalog is approximately $\sim$150 Mb (in ASCII format) and the table is available electronically with this paper.

As a useful reference for readers Table 3 provides 323 sources identified in the crossmatch between the GCK catalog and the *Kepler* targets with confirmed planetary companions. A segment of this table is illustrated in Table 5 and contains the information of columns 1–7, 10, 17, and 20–28 listed in Table 3.

The *Kepler* field observation was funded by Cornell University. M.O. wishes to express his gratitude to the Astronomy Group of the University of Rochester for their hospitality and to CONACyT for the financial support received through the "Beca Mixta" program. M.C., E.B., and M.O. also thank CONACyT for financial support through grants SEP-2009-134985 and SEP-2011-169554. E.E.M. acknowledges support from NSF award AST-1313029. We thank Chase Million for useful discussions. *GALEX* (*Galaxy Evolution Explorer*) is a NASA Small Explorer, launched in 2003 April. We gratefully acknowledge NASA's support for construction, operation, and science analysis for the *GALEX* mission, developed in cooperation with the Centre National d'Études Spatiales of France and the Korean Ministry of Science and Technology.

REFERENCES

Basri, G., Borucki, W. J., & Koch, D. 2005, NewAR, 49, 478
Bertin, E., & Arnouts, S. 1996, A&AS, 117, 393
Bianchi, L., Conti, A., & Shiao, B. 2014, AdSpR, 53, 900
Borucki, W. J., Koch, D. G., Lissauer, J. J., et al. 2003, Proc. SPIE, 4854, 129
Brown, T. M., Everett, M., Latham, D. W., & Monet, D. G. 2005, BAAS, 37, 110.12
Brown, T. M., Latham, D. W., Everett, M. E., & Esquerdo, G. A. 2011, AJ, 142, 112
Camarota, L., & Holberg, J. B. 2014, MNRAS, 438, 3111
do Nascimento, J.-D., Jr., García, R. A., Mathur, S., et al. 2014, ApJL, 790, L23
Everett, M. E., Howell, S. B., & Kinemuchi, K. 2012, PASP, 124, 316
Findeisen, K., Hillenbrand, L., & Soderblom, D. 2011, AJ, 142, 23
García, R. A., Ceillier, T., Salabert, D., et al. 2014, A&A, 572, A34
Greiss, S., Steeghs, D., Gänsicke, B. T., et al. 2012, AJ, 144, 24
Kawaler, S. D. 1988, ApJ, 333, 236
Latham, D. W., Brown, T. M., Monet, D. G., et al. 2005, BAAS, 37, 110.13
Lawrence, A., Warren, S. J., Almaini, O., et al. 2007, MNRAS, 379, 1599
Mamajek, E. E., & Hillenbrand, L. A. 2008, ApJ, 687, 1264
Martin, D. C., Fanson, J., Schiminovich, D., et al. 2005, ApJL, 619, L1
McQuillan, A., Mazeh, T., & Aigrain, S. 2014, ApJS, 211, 24
Meibom, S., Barnes, S. A., Platais, I., et al. 2015, arXiv:1501.05651
Mestel, L. 1968, MNRAS, 138, 359
Morrissey, P., Conrow, T., Barlow, T. A., et al. 2007, ApJS, 173, 682
Narain, U., & Ulmschneider, P. 1996, SSRv, 75, 453
Olmedo, M., Chávez, M., Bertone, E., & De la Luz, V. 2013, PASP, 125, 1436
Reinhold, T., Reiners, A., & Basri, G. 2013, A&A, 560, A4
Smith, M., & Shiao, B. 2011, BAAS, 43, 140.16
Ulmschneider, P., & Musielak, Z. 2003, in ASP Conf. Ser. 286, Current Theoretical Models and Future High Resolution Solar Observations: Preparing for ATST, ed. A. A. Pevtsov & H. Uitenbroek (San Francisco, CA: ASP), 363
Walkowicz, L. M., & Basri, G. S. 2013, MNRAS, 436, 1883

[11] http://mastweb.stsci.edu/kplrcasjobs/GOHelpKC.aspx